Molecular Crystals and Liquid Crystals
Publication details, including instructions for authors and subscription information:
http://www.tandfonline.com/loi/gmcl20

Surface-Groove-Induced Boundary-Roughness Effects in Nematics: A Comparison Between Models Allowing or Not Allowing Twist Deformation

Xuan Zhou [a b], Zhidong Zhang [c] & Li Xuan [a b]

[a] State Key Lab of Applied Optics, Changchun Institute of Optics, Fine Mechanics and Physics, Chinese Academy of Sciences, Changchun, Jilin, P. R. China

[b] Graduate School of the Chinese Academy of Sciences, Beijing, P. R. China

[c] Department of Physics, Hebei University of Technology, Tianjin, P. R. China

Version of record first published: 30 Jul 2012.

To cite this article: Xuan Zhou , Zhidong Zhang & Li Xuan (2012): Surface-Groove-Induced Boundary-Roughness Effects in Nematics: A Comparison Between Models Allowing or Not Allowing Twist Deformation, Molecular Crystals and Liquid Crystals, 562:1, 66-75

To link to this article: http://dx.doi.org/10.1080/15421406.2012.661312

Mol. Cryst. Liq. Cryst., Vol. 562: pp. 66–75, 2012

ISSN: 1542-1406 print/1563-5287 online
DOI: 10.1080/15421406.2012.661312

Surface-Groove-Induced Boundary-Roughness Effects in Nematics: A Comparison Between Models Allowing or Not Allowing Twist Deformation

XUAN ZHOU,[1,2] ZHIDONG ZHANG,[3,*]
AND LI XUAN[1,2]

[1]State Key Lab of Applied Optics, Changchun Institute of Optics, Fine Mechanics and Physics, Chinese Academy of Sciences, Changchun, Jilin, P. R. China
[2]Graduate School of the Chinese Academy of Sciences, Beijing, P. R. China
[3]Department of Physics, Hebei University of Technology, Tianjin, P. R. China

We investigate the boundary-roughness effect on nematics induced by a grooved surface based on two models composed of a lower grooved surface with homeotropic anchoring and an upper flat surface with planar anchoring, and the director at the upper surface is either perpendicular to the direction of grooves (model I) or parallel to it (model II). By comparison, we find that the effect of roughness on model II is larger than model I, which results from the twist deformation in model II. The effective anchoring strength in model II increases with the value of K_2/K_1. Moreover, the free energy of model I is lower than that of model II for nematics with K_2/K_1.

Keywords Effective tilt angle; extrapolation length; surface grooves; weak anchoring effect

Introduction

Inhomogeneous or nanotextured surface in nematic liquid crystal (NLC) cells has a significant effect on the alignment of liquid crystal (LC) molecules [1–6]. There have been many experimental attempts to achieve some desirable anchoring properties by surface tailored with microscopic grooves or geometrical patterns [7–10]. Those studies have been attracting attention because they propose novel methods of preparing anchoring surfaces different from conventional techniques such as surface rubbing. Recently, the experimental realization of a submicrometer-scale surface grooved with sufficient geometrical precision has provoked interest in the effects of rough surface [11–20].

Experiments [14–16], theory [17], as well as simulations [18,19] have shown that rough or nanotextured surface can reduce the order close to the surface, and nucleate a boundary layer of strongly reduced order, which is called "surface melting" [20]. Within the boundary layer where the nematic order decreases, the director changes rapidly and gives rise to a nontrivial structure [20].

*Address correspondence to Zhidong Zhang, Department of Physics, Hebei University of Technology, Tianjin 300401, P. R. China. E-mail: zhidong_zhang@yahoo.cn

The combined effect of rapidly varying director anchoring and surface melting gives rise to an effective weak anchoring effect [20,21]. The problem of relating the effective anchoring extrapolation length to the microscopic roughness parameters has been studied in several theoretical papers, framed within the Frank theory [22–24] or the Landau-de Gennes theory [20].

However, all of the analytic arguments are based on an assumption that the surface slope and the resultant distortion are small enough so that it is sufficient to consider the quadratic form of the Frank elastic energy in terms of the director distortion. Therefore, numerical studies will be inevitable to understand the properties of grooved surfaces with relatively large slopes. Although there have been a number of numerical studies to elucidate the behavior of NLC in the vicinity of a grooved surface [25–27], few of them aimed at the roughness effects of such surfaces, especially the models with twist deformation in the bulk.

In this paper, we analyze in numerical detail the boundary-roughness effects induced by grooved surfaces with relatively large slopes by the two-dimensional finite-difference iterative method [28]. We set ourselves within the Frank elastic theory, in which the order parameter S of the NLC is assumed uniform and equal to the bulk value S_B, and only the director $\vec{n}$ varies in space [14]. Reference [20] gives the elastic constants K_i depending on S in the form $K_1 = K_3 = 2S_B^2(L_1 + L_2 + L_3)$, $K_2 = 2S_B^2 L_1$. Our results confirm the effective weak anchoring effects already obtained in Ref. [20] and show some new phenomena, such as the twist effect of the grooved surfaces.

The Model

In order to study the weak anchoring effect of grooved surfaces, we propose two NLC models composed of a grooved surface and a flat surface, as shown in Figs. 1(a) and (b), which we referred to as model I and model II, respectively.

The direction of the grooves is assumed to be parallel to the y-axis of a Cartesian reference frame and assumes uniformity along this direction ($\partial/\partial y = 0$). The height of the surface with respect to a reference plane $z = 0$ is assumed to be given by a cosine function

$$z_0(x) = A[\cos(qx) - 1], \tag{1}$$

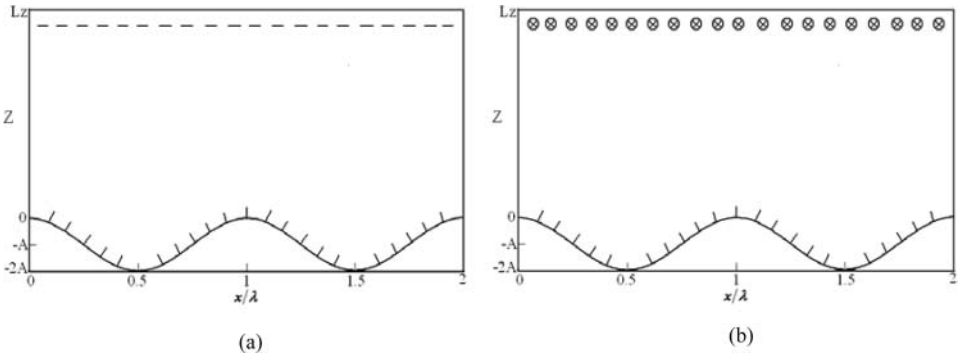

Figure 1. Schematic representation of two NLC models composed of a grooved surface and a flat surface. (a) Model I: The top flat surface with planar anchoring perpendicular to the direction of grooves. (b) Model II: The top flat surface with planar anchoring parallel to the direction of grooves.

where $q = 2\pi/\lambda$ is the wave vector of the surface grooves, λ is the spatial periodicity of the grating surface, and A is its amplitude. At this lower surface, we enforce a strong homeotropic anchoring, where the director $\vec{n}$ orients along the local surface normal $\vec{\nu}$, i.e., $\vec{n}//\vec{\nu}$.

At the upper plane surface $z = L_z$, we assume a strong planar anchoring condition. The director $\vec{n}$ at the surface is either perpendicular to the direction of grooves [Fig. 1(a)] or parallel to it [Fig. 1(b)]. As $Aq \to 0$, both models reduce to hybrid-aligned nematic (HAN) cell. In model I, the wave vector is in the HAN plane, hence the distortion induced by the grooved surface and the uniform deformation are in the same plane; while in model II, the wave vector is perpendicular to the HAN plane, hence the distortion induced by the grooved surface and the uniform deformation are not in the same plane. In other words, model I allows twist deformation in the bulk while model II does not.

Numerical Methods

In our numerical system, we assume a periodic boundary condition along the x direction, so that the director profile satisfies $\vec{n}(x, z) = \vec{n}(x + m\lambda, z)$, with m being an arbitrary integer. The area of our numerical system in the (x, z) space is described by $0 \le x < \lambda$ and $z_0(x) \le z \le L_z$.

We introduce the new dimensionless coordinate $\tilde{x} = \frac{x}{\lambda}$, $\tilde{z} = \frac{z}{L_z+2A}$ and define the dimensionless parameters $\tilde{A} = \frac{A}{L_z+2A}$, $\tilde{L}_z = \frac{L_z}{L_z+2A}$, $\tilde{\lambda} = \frac{\lambda}{\lambda}$, and $\tilde{q} = \frac{2\pi}{\tilde{\lambda}} = q\lambda$, thus the system described by $x \in [0, \lambda)$, $z \in [-2A, L_z]$ in the (x, z) space is mapped onto a scaled space: $\tilde{x} \in [0, 1)$, $\tilde{z} \in [-2\tilde{A}, \tilde{L}_z]$. The numerical calculations are to be intended with respect to the scaled variables.

The total free energy per unit area of the surface is given by

$$F = \frac{1}{\lambda}\int_0^{\lambda} d\tilde{x}\frac{\partial x}{\partial \tilde{x}}\int_{z_0}^{L_z} d\tilde{z}\frac{\partial z}{\partial \tilde{z}} f_{\text{Frank.}}\left\{\vec{n},\, \partial_{\tilde{x}}\vec{n}\,(\tilde{x}, \tilde{z})\,,\, \partial_{\tilde{z}}\vec{n}\,(\tilde{x}, \tilde{z})\right\}. \tag{2}$$

We discretize the scaled space $(\tilde{x}, \tilde{z})$ by 400×401 grid points with equal grid spacing, i.e., $\Delta\tilde{x} = \Delta\tilde{z} = 0.0025$, which has been demonstrated sufficient to get the reasonable and relatively accurate result. The director $\vec{n}$ at each grid point is assigned as $\vec{n}_{i,k} = \vec{n}(\tilde{x}_i, \tilde{z}_k)$ with $\tilde{x}_i = (i-1)\Delta\tilde{x}$, $\tilde{z}_k = (k-1)\Delta\tilde{z} - 2\tilde{A}$, $i \in [1, 400]$, and $k \in [1, 401]$. We adopt periodic boundary conditions in the x direction that conform to the periodicity of the surface. Here, we do not detail the discretization of Eq. (2). We merely mention that F is expressed as the sum of the contributions from each cell $[(i-1)\Delta\tilde{x} \le i\Delta\tilde{x} \le (i+1)\Delta\tilde{x}, (k-1)\Delta\tilde{z} \le k\Delta\tilde{z} \le (k+1)\Delta\tilde{z}]$, in which $f_{\text{Frank}}(i, k)$ is a function of $\vec{n}_{i,k}$, $\vec{n}_{i+1,k}$, $\vec{n}_{i-1,k}$, $\vec{n}_{i,k+1}$, and $\vec{n}_{i,k-1}$.

For each point $(\tilde{x}_i, \tilde{z}_0(\tilde{x}_i))$ of the grooved surface, there is a corresponding J_i determined by $|\tilde{z}_{j_i} - \tilde{z}_0(\tilde{x}_i)| < \frac{\Delta\tilde{z}}{2}$, where $\tilde{z}_{j_i} = (j_i - 1)\Delta\tilde{z} - 2\tilde{A}$ and $\tilde{z}_0(\tilde{x}_i) = \tilde{A}[\cos\tilde{q}\tilde{x}_i - 1] = \tilde{A}[\cos q x_i - 1]$, with $x_i = (i-1)\Delta x$ and $\Delta x = \frac{\lambda}{400}$. We let the system relax from an initial condition under the fixed boundary condition at the upper surface $[\vec{n}_{i,401} = (1, 0, 0)]$ (model I) or $[\vec{n}_{i,401} = (0, 1, 0)]$ (model II), and the homeotropic boundary condition at the lower surface $(\vec{n}_{i,j_i}//\vec{\nu}_i)$, where $\vec{\nu}_i$ is the local surface normal at $(x_i, z_0(x_i))$ in the real (x, z) space.

We employ

$$-\gamma_1\frac{\partial\vec{n}}{\partial t} = \left(\vec{n}\cdot\frac{\delta F}{\delta\vec{n}}\right)\vec{n} - \frac{\delta F}{\delta\vec{n}}, \tag{3}$$

as the relaxation equation to iterate the director simulation [29], where $\frac{\delta F}{\delta \vec{n}} = \nabla \cdot \frac{\partial f}{\partial \nabla \vec{n}} - \frac{\partial f}{\partial \vec{n}}$ and the Lagrange multiplier term is dropped. To discretize Eq. (3), we replace the derivatives with finite-difference as follow:

$$-\gamma_1[\vec{n}\,(t+\Delta t) - \vec{n}\,(t)]/\Delta t = \left(\vec{n}\,(t) \cdot \frac{\delta F}{\delta \vec{n}\,(t)}\right)\vec{n}\,(t) - \frac{\delta F}{\delta \vec{n}\,(t)}. \tag{4}$$

After the director is updated, we renormalize it back to unit length by dividing the total length of the updated vector, as shown in Eq. (5)

$$\vec{n}(t+\Delta t) \Leftarrow \frac{\vec{n}(t+\Delta t)}{|\vec{n}(t+\Delta t)|}. \tag{5}$$

In our numerical calculations, we have found that a discretization with time step given by 10^{-7} is sufficient to guarantee the stability of the numerical procedure. In addition, our equilibration runs take 50×10^4, which has been confirmed sufficient for the system to reach equilibrium state.

We calculate the tilt angle distribution and the total elastic energy of the two models after the system reaching equilibrium. In order to make the calculation of the tilt angle easier, we approximately consider $z = 0$ in Fig. 1 as effective flat boundary, and the rationality of this approximation will be discussed in the conclusion part. At each layer above $z = 0$, we have calculated the tilt angle $\vartheta_/ = \tan^{-1}(\bar{n}_x/\bar{n}_z)$ for model I and $\vartheta_/ = \tan^{-1}(\bar{n}_y/\bar{n}_z)$ for model II, where $\bar{n}_x$, $\bar{n}_y$, and $\bar{n}_z$ are the average values of each component of the director, and the average is performed over all particles of a period in the layer, i.e., $i \in [1, 400]$. Here, we notice that $\vartheta_/$ and $\vartheta_{//}$ characterize the deviation from z-axis in each HAN plane of the two models.

We choose the material parameters $K_1 = K_3 = K = 8.11 \times 10^{-12} N$ and $K_s/K_3 = 1$. The former conforms to the inequality $K_2 < K_1 \leq K_3$ fulfilled by most rod-like nematics [30], and $K_s/K_3 = 1$ is the largest value allowed in the equality $K_{24} \leq K_1$ or K_2 guaranteeing the positive definiteness of the Frank elastic energy [31,32]. We should notice that the surface-like elastic constant K_s does not present in the relaxation equation, i.e., Eq. (3), therefore, surface-like elasticity will not influence the director profile; but it will contribute to the elastic energy for the two models we proposed, due to the lower rough surface.

In our numerical calculations, we choose $A = 0.1\,\mu m$ and $L_z = 0.8\,\mu m$ and make the two values constant. In order to change the value of Aq, we make the wave vector $q = 2\pi/\lambda$ vary, i.e., the spatial periodicity λ varies. As geometrical parameters, we choose $Aq = 0.2\pi (\approx 0.628)$, $0.4\pi (\approx 1.256)$, and $0.5\pi (\approx 1.57)$, which are of order unity.

Results and Discussions

According to the values of A and L_z, we have $\tilde{A} = 0.1$ and $\tilde{L}_z = 0.8$, i.e., $\tilde{L}_z/\tilde{A} = 8$ and $\tilde{z} \in [-0.2, 0.8]$. From $\tilde{z}_k = (k-1)\Delta\tilde{z} - 2\tilde{A}$, we can easily get that the layer $k = 81$ corresponds to the effective flat boundary $z = 0$, i.e., $\tilde{z}_{81} = 0$. Above $z = 0$, there are 320 layers, which is sufficient to capture the behavior of the directors correctly.

Under one elastic constant approximation ($K_1 = K_2 = K_3 = K$), the curves of tilt angle ($\vartheta_/$, $\vartheta_{//}$) for $Aq = 0.2\pi,\ 0.4\pi$, and 0.5π as a function of z are shown in Fig. 2. It is shown that in both the two models, the grooved surface causes a nonzero effective boundary tilt angle [$\vartheta_/(0)$ and $\vartheta_{//}(0)$] at the effective flat surface $z = 0$, and the values of $\vartheta_/(0)$ and $\vartheta_{//}(0)$ increase with the value of Aq. The results are consistent with the analytical results reported in Ref. [20], which investigated the boundary-roughness effects in a nematic cell

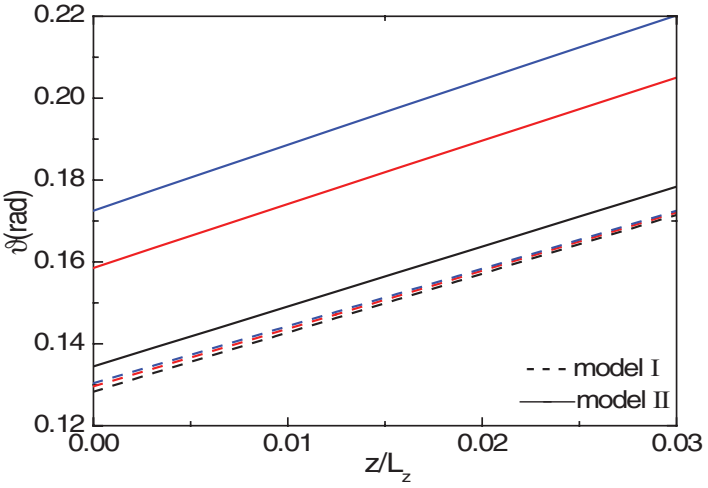

Figure 2. (Color online) Tilt angle profiles against distance z for model I (dashed line) and Model II (solid line). From bottom to top, the values of Aq are 0.2π, 0.4π, and 0.5π, respectively.

similar to model I, framed within the Landau-de Gennes theory. According to our numerical results and the analytical results in Ref. [20], we can infer that, the effective tilt angles $\vartheta_{/}(0)$ and $\vartheta_{//}(0)$ trend to zero as $Aq \to 0$, in other words, both the two models reduce to HAN cell, and the energy of the two models are almost equal, which is consistent with the theoretical results in Appendix A.

From the data given in Fig. 2, we get the extrapolation lengths corresponding to $Aq = 0.2\pi,\ 0.4\pi$, and 0.5π are b/A $= 0.712$, 0.719, 0.724 (model I) and b/A $= 0.749$, 0.898, 0.987 (model II), respectively. According to $b = K/W$, we conclude that the effective anchoring strength decreases with the value of Aq. According to the actual amplitude A of surface grooves $[(10^{-8}\sim10^{-7})m]$, we obtain the effective anchoring strength $W\sim(10^{-3}\sim10^{-4})J/m^2$, which is reasonable.

Figure 2 also shows that the effective boundary tilt angle of model I $\vartheta_{/}(0)$ is always bigger than that of model II $\vartheta_{//}(0)$ at certain Aq, meaning that the effective anchoring strength of model I is always weaker than that of model II; and the difference between $\vartheta_{/}(0)$ and $\vartheta_{//}(0)$ increases with the value of Aq. The results are caused by the twist effect in model I, and the presence of n_x component in model II indicates this effect (see Fig. 3). We notice that the tilt angle $\vartheta_{=}\tan^{-1}(\bar{n}_y/\bar{n}_z)$ is defined in HAN plane, whereas the polar angle respect to the $x-y$ plane is $\theta_{=}\tan^{-1}(\sqrt{(\bar{n}_y^2+\bar{n}_x^2)}/\bar{n}_z)$.

Figure 3 gives the plot of $\bar{n}_x$ component of the director in model II for different values of Aq, where the average is performed over half a period in the layer, i.e., $i \in [1, 201]$, in order to avoid plus–minus offset. We find that as Aq increases, the $\bar{n}_x$ component becomes bigger and the relaxation becomes slower significantly, which directly induces the increase of twist energy. The deformation of model II has to overcome more twist energy, and the surface anchoring decreases, which is denoted by the increase of anchoring extrapolation length or the increase of effective boundary tilt angle $\vartheta_{//}(0)$.

In order to further study the effect of twist deformation in model I, we introduce a dimensionless parameter $\tau = K_2/K_1$, then we plot the tilt angle $\vartheta_{//}$ and the $\bar{n}_x$ component of the director for $\tau = 0.5,\ 0.8$, and 1.0 at $Aq = 0.2\pi$, as shown in Fig. 4. It is shown in

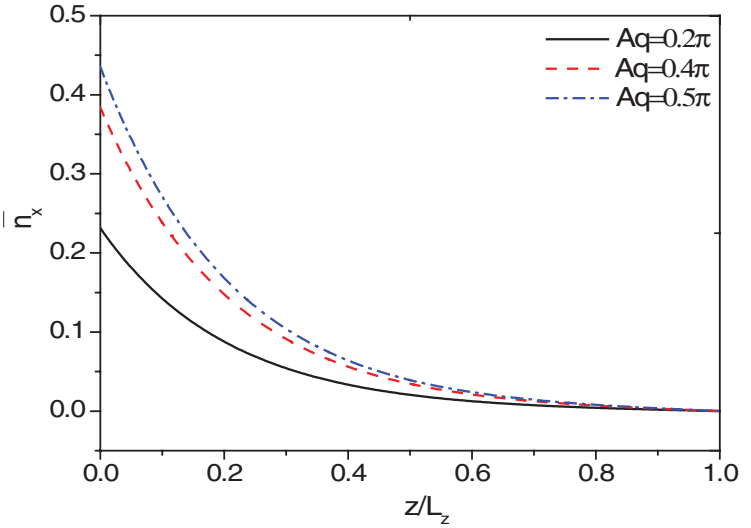

Figure 3. (Color online) The plot of $\bar{n}_x$ component of director in model II. The values of Aq are 0.2π, 0.4π, and 0.5π (solid line, dashed line, and dash dot line), respectively.

Fig. 4(a) that the effective boundary tilt angle $\vartheta_{//}(0)$ decreases as the value of τ increases, and it can be illustrated by Fig. 4(b), which shows that as τ increases, the $\bar{n}_x$ component becomes smaller.

We plot in Fig. 5, the energy of two models as a function of τ for $Aq = 0.2\pi$. The energy here is the total Frank elastic energy per unit area. It is shown that the energy of model I increases with τ; while the energy of model II remains unvaried. Moreover, the energy of model I is always lower than that of model II for nematics with $\tau < 1\,(K_2 < K_1)$, as is the case for most nematics. This result is in agreement with the analytic results in Appendix A.

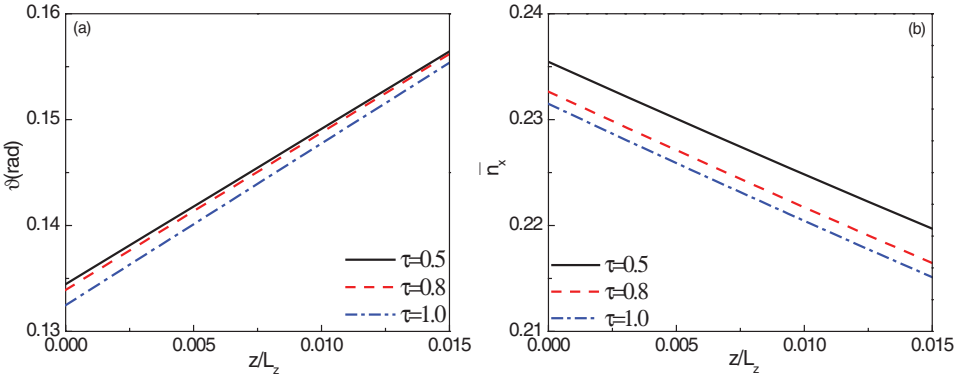

Figure 4. (Color online) The director profiles of model II at $Aq = 0.2\pi$ for different values of $\tau = 0.5$, 0.8, and 1.0 (solid line, dashed line, and dash dot line), respectively. (a) Tilt angle profiles $\vartheta_{//}$. (b) $\bar{n}_x$ component of director.

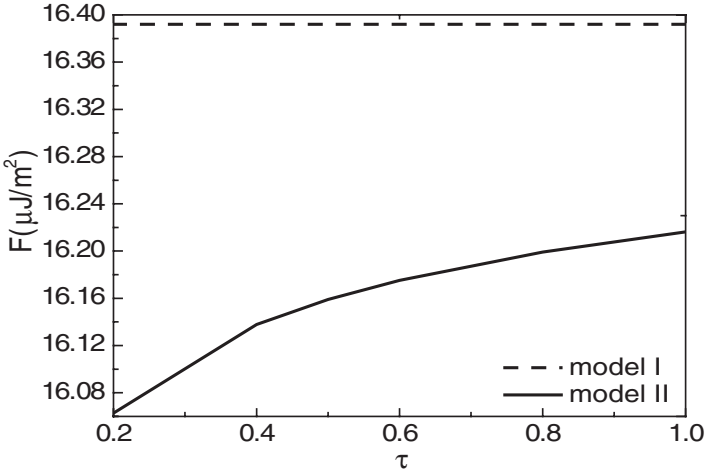

Figure 5. Frank elastic energy per unit area as a function of $\tau = K_2/K_1$ for $Aq = 0.2\pi$.

Conclusion

To investigate the boundary-roughness effects on nematics induced by a grooved surface, we have performed numerical calculations of the equilibrium distribution and the total Frank elastic energy of two models, composed of a lower grooved surface with relatively large amplitude A and homeotropic anchoring and an upper flat surface with planar degenerate anchoring, where the director is either perpendicular to the direction of grooves (model I) or parallel to it (model II).

The extrapolation length $b = K/W$ serves as a measure of the effective anchoring strength. Our results confirm the weak anchoring effect reported in Ref. [20], i.e., the effective anchoring strength decreases as the value of Aq increases. By comparison between the two models, we find that the effect of roughness on model II is larger than model I and the effective anchoring strength in model II increases with the value $\tau = K_2/K_1$, which result from the twist effect in model II. Further, the energy of model II is always lower than that of model I for nematics with $\tau < 1$. Combined with the analytic result in Appendix A, we conclude that for a nematic cell composed of a lower grooved surface with homeotropic anchoring and a planar degenerate upper surface, it will nonetheless tend to align the nematic with $K_2 < K_1$ on the upper surface along the direction of the grooves, as model II has the minimum energy.

In the numerical calculations of tilt angle, we have introduced an effective flat boundary, i.e., the plane $z = 0$. In order to illustrate its rationality, we consider a submicrometer-scale surface groove [$\lambda \sim 10^{-7}m$ and $A \sim (10^{-8} \sim 10^{-7})m$]. Compared with the actual cell thickness in practical application ($\geq 2 \times 10^{-6}m$), the amplitude A is comparatively small and a distance of $2A$ from the actual lower surface (see Fig. 1) will not influence the result. Therefore, we consider the reference plane $z = 0$ as effective flat boundary to simplify our calculation. Here, we emphasize that this approximation is appropriate only when the amplitude A of the grooves is much smaller than the cell thickness, and it only used for the calculation of tilt angle, while the calculation of elastic energy is performed over the whole numerical system.

The anchoring energy calculated numerically is qualitatively consistent with analytical ones, even when Aq is of order unity. Considering the assumption of $Aq << 1$ in deriving the analytical anchoring energy, our findings are somewhat surprising, and it indicates that the analytical theory can describe the qualitative feature of the anchoring of grooved surfaces in spite of the assumption $Aq << 1$ does not hold.

We should notice that in our analysis, we have compared approximate analytical solutions with the "exact" one, given by numerical calculations with the correct boundary conditions. While in the analytical process, we have introduced some approximations, such as the approximate lower surface boundary, no azimuthal director distortion, and neglecting the contribution of the surface-like elasticity. It has been proved that these approximations have strong influence on the correct evaluation of the anchoring energy [11–13], thus the consistent is only an approximate and qualitative conclusion.

Acknowledgments

This research was supported by Natural Science Foundation of Hebei Province under Grant No. A2010000004 and National Natural Science Foundation of China under Grants No. 60736042, and Key Subject Construction Project of Hebei Province University. The authors would like to thank the anonymous reviewers for their insightful comments, which have greatly improved the quality of this article.

Appendix A: Analytic Solutions

The Frank elastic energy density of a nematic LC can be described in terms of $\vec{n}$ as [30]

$$f = \frac{1}{2}\left[K_1 (\nabla \cdot \vec{n})^2 + K_2 (\vec{n} \cdot \nabla \times \vec{n})^2 + K_3 (\vec{n} \times \nabla \times \vec{n})^2\right], \tag{A.1}$$

where K_1, K_2, K_3 are the elastic constants associated with splay, twist, and bend distortions, respectively.

On the assumption that $Aq \ll 1$, the azimuthal director distortion is negligibly small and the director $\vec{n}$ can be considered to be constrained to a single plane that makes an azimuthal angle ϕ with the wave vector of the grooves, thus $\vec{n}$ can be expressed as

$$\vec{n} = (\sin\theta\cos\phi, \sin\theta\sin\phi, \cos\theta), \tag{A.2}$$

where $\theta = \theta(x, z)$. After making the simplification that $K_1 = K_3 = K$, the bulk free energy density is

$$f = \frac{1}{2}K\left[\kappa\left(\theta_{,x}\right)^2 + \left(\theta_{,z}\right)^2\right], \tag{A.3}$$

where $\theta_{,x} = \partial\theta/\partial x$, $\theta_{,z} = \partial\theta/\partial z$, $\kappa = 1 - (1-\tau)\sin^2\phi$, and $\tau = K_2/K_1$. The Euler-Lagrange equation is

$$\kappa\theta_{,xx} + \theta_{,zz} = 0. \tag{A.4}$$

In the theoretical treatment, we introduce the same approximation as Ref. [20], i.e., we replace the lower grooved surface by an undulating boundary condition on an effective flat surface ($z = 0$ in Fig. 1), i.e.,

$$\theta(x, 0) = Aq\sin(qx), \tag{A.5}$$

and the boundary condition on the upper surface ($z = L_z$) is

$$\theta(x, L_z) = \frac{\pi}{2}. \tag{A.6}$$

Equations (A.4)–(A.6) admit the simple solution

$$\theta(x, z) = \frac{\pi}{2}\frac{z}{L_z} + Aq\sin(qx)e^{-q\sqrt{\kappa}z}. \tag{A.7}$$

Equation (A.7) satisfies Eqs. (A.4) and (A.5) strictly, while it satisfies Eq. (A.6) approximately on the assumption $\frac{L_z}{A} >> 1$. Substituting Eq. (A.7) in to Eq. (A.3) and integrating over x and z yields the bulk free energy per unit area as

$$F = \frac{1}{4}K\sqrt{\kappa}A^2q^3 + \frac{\pi^2 K}{8L_z}, \tag{A.8}$$

in which the first term is surface-groove-induced azimuthal anchoring energy and the second one is the energy of uniform HAN deformation. We should notice that in our analytic process, the surface-like elasticity is omitted, just because we cannot get a reasonable solution about it under the assumption of no azimuthal distortions, not because it does not contribute to the free energy.

From Eq. (A.8), we find that for model I, $\phi = 0$ and $\kappa = 1$, $F_{/} = \frac{1}{4}KA^2q^3 + \frac{\pi^2 K}{8L_z}$; while for model II, $\phi = \frac{\pi}{2}$ and $\kappa = \tau$, $F_{//} = \frac{1}{4}K\sqrt{\tau}A^2q^3 + \frac{\pi^2 K}{8L_z}$. The expressions of $F_{/}$ and $F_{//}$ show that

1. When $Aq \to 0$, the energy of the two models are almost equal, i.e., $F \to \frac{\pi^2 K}{8L_z}$, representing the uniform HAN configuration.
2. The energy of model I ($F_{//}$) increases with τ, while that of model II ($F_{/}$) remains constant.
3. If $\tau < 1$ ($K_2 < K_1$), Eq. (A.8) has a minimum at $\phi = \frac{\pi}{2}$, which corresponds to model I, and a maximum at $\phi = 0$ which corresponds to model II. It is possible then if the upper surface $z = L_z$ is planar degenerate anchoring, it will nonetheless tend to align a nematic with $K_2 < K_1$ along the direction of the grooves, in other words, the NLC cell forms the configuration of model I, as model I has the minimum energy. This mechanism requires anisotropic elastic constants and is somewhat similar to the result in Ref. [33].

References

[1] Cognard, J. (1982). *Mol. Cryst. Liq. Cryst.*, Suppl. Ser., *A5*, 1.
[2] Stöhr, J., Samant, M. G., Lüning, J., Callegari, A. C., Chaudhari, P., Doyle, J. P., Lacey, J. A., Lien, S. A., Purushothaman, S., & Speidell, J. L. (2001). *Science*, *292*, 2299.
[3] Bryan-Brown, G. P., Brown, C. V., Sage, I. C., & Hui, V. C. (1998). *Nature (London)*, *392*, 365.
[4] Newsome, C. J., O'neill, M., Farley, R. J., & Bryan-Brown, G. P. (1998). *Appl. Phys. Lett.*, *72*, 2078.
[5] Lu, X., Lee, F. K., Sheng, P., Kwok, H. S., Chigrinov, V., & Tsui, O. K. C. (2006). *Appl. Phys. Lett.*, *88*, 243508.
[6] Yeung, F. S. Y., Xie, F.-C., Wan, J. T.-K., Lee, F. K., Tsui, O. K. C., Sheng, P., & Kwok, H.-S. (2006). *J. Appl. Phys.*, *99*, 124506.
[7] Rüetschi, M., Grütter, P., Fünfschilling, J., & Güntherodt, H.-J. (1994). *Science*, *265*, 512.
[8] Kim, J.-H., Yoneya, M., Yamamoto, J., & Yokoyama, H. (2001). *Appl. Phys. Lett.*, *78*, 3055.

[9] Zhang, B., Lee, F. K., Tsui, O. K. C., & Sheng, P. (2003). *Phys. Rev. Lett.*, *91*, 215501.
[10] Gwag, J. S., Fukuda, J., Yoneya, M., & Yokoyama, H. (2007). *Appl. Phys. Lett.*, *91*, 073504.
[11] Barbero, G., Gliozzi, A. S., Scalerandi, M., & Evangelista, L. R. (2008). *Phys. Rev. E*, *77*, 051703.
[12] Barbero, G., Gliozzi, A. S., & Scalerandi, M. (2008). *J. Appl. Phys.*, *104*, 094903.
[13] Fukuda, J., Yoneya, M., & Yokoyama, H. (2007) *Phys. Rev. Lett.*, *99*, 139902.
[14] Barberi, R., & Durand, G. (1990). *Phys. Rev. A*, *41*, 2207.
[15] Papanek, J., & Martinot-Lagarde, Ph. (1996). *J. Physique II France*, *6*, 205.
[16] Wen, B., Kim, J., Yokoyama, H., & Rosenblatt, C. (2002). *Phys. Rev. E*, *66*, 041502.
[17] Barbero, G., & Durand, G. (1991). *J. Phys. II*, *1*, 651.
[18] Cheung, D. L., & Schmod, F. (2005). *J. Chem. Phys.*, *122*, 074920.
[19] Cheung, D. L., & Schmod, F. (2006). *Chem. Phys. Lett.*, *418*, 392.
[20] Turzi, S. (2007). Distortion-induced effects in nematic liquid crystals. PhD thesis, Politecnico di Milano, Italy.
[21] Sato, Y., Sato, K., & Uchida, T. (1992). *Jap. J. Appl. Phys. Lett.*, *31*, L579.
[22] Alexe-Ionescu, A. L., Barberi, R., Barbero, G., & Giocondo, M. (1994). *Phys. Rev. E*, *49*, 5378.
[23] Evangelista, L. R., & Barbero, G. (1993). *Phys. Rev. E*, *48*, 1163.
[24] Fournier, J. B., & Galatola, P. (2000). *Eur. Phys. J. E*, *2*, 59.
[25] Patrício, P., Telo da Gama, M. M., & Dietrich, S. (2002). *Phys. Rev. Lett.*, *88*, 245502.
[26] Parry-Jones, L. A., & Elston, S. J. (2005). *J. Appl. Phys.*, *97*, 093515.
[27] Spencer, T. J., & Care, C. M. (2006). *Phys. Rev. E*, *74*, 061708.
[28] Mori, H., Gartland, E. C., Kelly, J. R., & Bos, P. (1999). *Jpn. J. Appl. Phys.*, *38*, 135.
[29] Anderson, J. E., Watson, P. E., & Bos, P. E. (2001). *LC3D: Liquid Crystal Display 3-D Director Simulator Software and Technology Guide*, Chapter 3, Artech House: London.
[30] de Gennes, P. J., & Prost, J. (1993). *The Physics of Liquid Crystals*, Oxford University Press: Oxford.
[31] Virga, E. G. (1994). *Variational Theories for Liquid Crystals*, Chapman and Hall: London.
[32] Ericksen, J. L. (1966). *Phys. Fluids*, *9*, 1205.
[33] Atherton, T. J., & Sambles, J. R. (2006). *Phys. Rev. E*, *74*, 022701.